Nano Research

Open Access

Research Article

Fe-N_2 single-atom sites unlocked ligand-to-metal charge transfer in semiconductor photocatalytic decarboxylation

Yu Jiang, Guanglin Wang, Menglong Ma, Jinming Wang, Li An, Dan Qu, Kun Zheng, Peijie Ma ✉, Yichang Liu ✉, and Zaicheng Sun ✉

Center of Excellence for Environmental Safety and Biological Effects, Beijing Key Laboratory for Green Catalysis and Separation, Department of Chemistry, College of Chemistry and Life Science, Beijing Key Laboratory of Microstructure and Property of Solids, College of Materials Science and Engineering, Beijing University of Technology, Beijing 100124, China

Cite this article: *Nano Research*, **2026**, *19*, 94908469. https://doi.org/10.26599/NR.2026.94908469

ABSTRACT: The outer-sphere single-electron transfer (SET) is the main pathway for activating substrates during semiconductor photocatalysis, which is limited by energy band structure and excited-state lifetime. Under light irradiation, the inner-sphere ligand-to-metal charge transfer (LMCT) from substrate to metal species can break through the above limitations and be complementary to the SET process. However, this LMCT activation mode has rarely been involved in heterogeneous semiconductor photocatalysis. Herein, we build Fe-N_2 single atom sites on carbon nitride (Fe-N_2/CN) and achieve the photocatalytic decarboxylative Giese reaction via radical–radical cross-coupling (up to 99% yields). This Fe-N_2/CN photocatalyst has both LMCT and SET activity, which could activate carboxylic acids and electron-deficient alkenes simultaneously. The carboxylic acid could coordinate with Fe sites and convert into alkyl radical via photo-induced LMCT decarboxylation pathway. Meanwhile, the electron-deficient olefins could be activated to radical anion through single-electron reduction by electrons in the conduction band of carbon nitride. Combining the LMCT and SET strategy opens a new avenue for the design of semiconductor catalysts, expanding the scope of photocatalytic redox reactions.

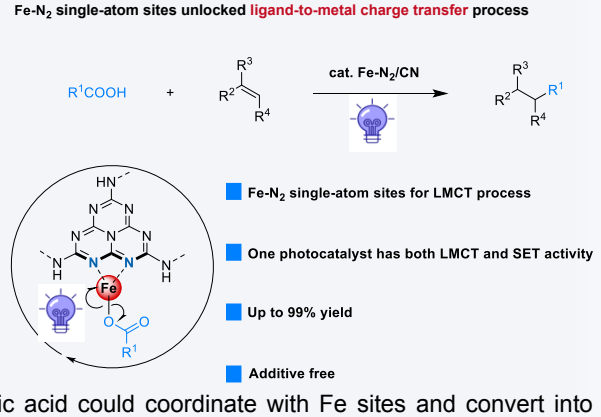

KEYWORDS: single-atom catalysis, ligand-to-metal charge transfer, iron catalysis, decarboxylative Giese reaction

1 Introduction

Photocatalysis, recognized as a sustainable and green method for organic synthesis, offers novel opportunity different from conventional ground-state catalysis [1–7]. The out-sphere single-electron transfer (SET) between photoexcited catalysts and substrates serves as the dominant mechanism for photocatalytic redox reactions in heterogeneous semiconductor catalysis (left of Fig. 1(a)) [8–10]. The efficiency of this process is largely governed by the energy band structure and excited-state lifetime of the photocatalyst, both of which have been extensively investigated [11–13]. The reactions are hard to take place when the redox potential of substrates are beyond that of photocatalysts. Recently, a photo-induced inner-sphere electron transfer process from ligand centered orbital to metal centered orbital has been proposed in homogeneous photocatalysis (right of Fig. 1(a)) [14–17]. This ligand-to-metal charge transfer (LMCT) pathway could break limitations of redox potential and excited-state lifetime, complementing with the SET process. In the LMCT, the type of metal center and ligand effect determine the catalytic performance.

Carboxylic acid groups are one of the most ubiquitous functionalities in organic molecules, affording the advantage of commercial availability [18]. Decarboxylative Giese reactions represent a powerful strategy for constructing $C(sp^3)$–$C(sp^3)$ bonds [19]. Due to the rapid addition rate of C-centered radicals to electron-deficient alkenes, which can reach up to 10^6 $M^{-1}\cdot s^{-1}$ [20], Giese reactions exhibit excellent functional group compatibility. Moreover, decarboxylative Giese reactions offer distinct site selectivity, making them an important protocol in the synthesis of

Received: November 7, 2025; **Revised:** December 28, 2025
Accepted: January 21, 2026

✉Address correspondence to Peijie Ma, peijiema@bjut.edu.cn; Yichang Liu, yichangliu@bjut.edu.cn; Zaicheng Sun, sunzc@bjut.edu.cn

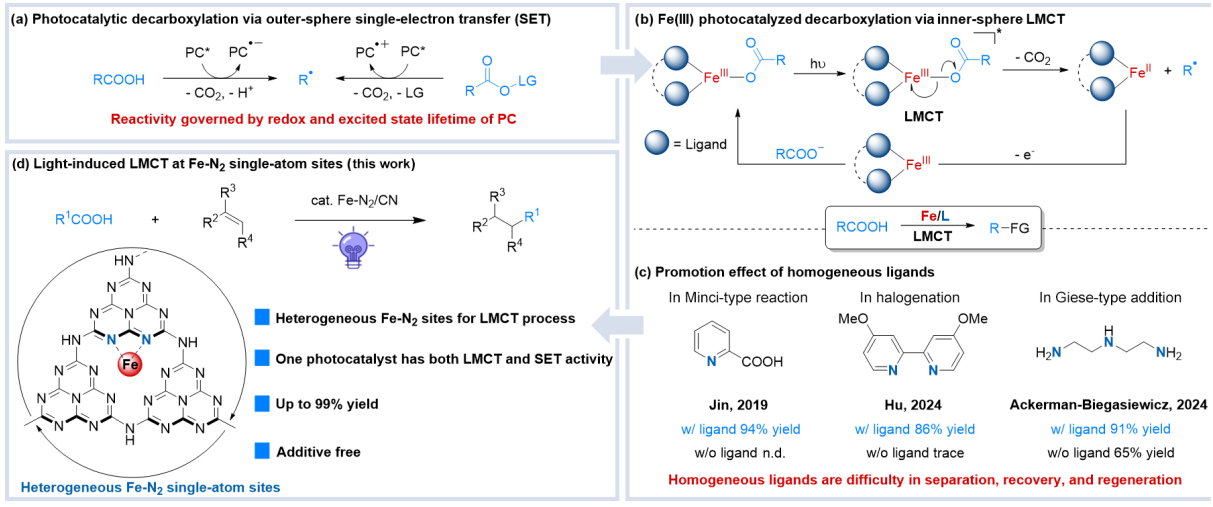

Figure 1 (a) Outer-sphere SET process in photocatalytic decarboxylation. (b) Light-induced inner-sphere LMCT process via Fe(III) catalysis. (c) The promotion effect of homogeneous ligands in Fe-catalyzed decarboxylative functionalization. FG, functional group. w/, with. w/o, without. (d) This work: Heterogeneous Fe-N_2 sites to promote LMCT in photocatalytic decarboxylative Giese reactions.

natural products and pharmaceuticals [21]. The unique redox activity of photochemistry provides a mild and green pathway for decarboxylation. Under photocatalysis, the direct oxidation of carboxylic acids or reduction of carboxylic acid derivatives, such as redox-active esters, enables the generation of the corresponding alkyl radicals for functionalization reactions [22–24]. However, the high oxidation potential of alkyl carboxylic acids poses challenges in terms of functional group tolerance. On the other hand, the use of carboxylic acid derivatives reduces both atom economy and step economy. Over the past decade, the LMCT process has provided another feasible route for direct decarboxylation of carboxylic acids, which can overcome redox potential limitation of substrates. After carboxylic groups coordinate with metal species, the homolytic cleavage of the M–O bond occurs under photoexcitation, releasing carboxyl radicals and then achieving decarboxylation (Fig. 1(b)). Ce(IV) [25, 26], Cu(II) [27, 28] and Fe(III) [29–35] have been demonstrated to catalyze the LMCT process in decarboxylative functionalization.

Among them, Fe is abundant in the earth's crust and characterized by low toxicity and inexpensive. In previous reports, the Fe-catalyzed LMCT processes were significantly influenced by ligand effects. With the addition of homogeneous nitrogen ligands such as pyridine [32], bipyridine [30], and diethylenetriamine [29] enhancing catalytic performance (Fig. 1(c)). However, homogeneous ligands are hard to recovery and reuse, and also complicate product separation and purification.

In single-atom site catalysts (SASCs), the isolated metal active sites with quasi-homogeneous coordination environment could be constructed on the surface of heterogeneous support [36–39] Combining single-atom catalysis with LMCT process, the light-induced decarboxylative functionalization might be realized in heterogeneous catalytic system. However, thus far, the photo-induced LMCT mechanism has rarely been involved in single-atom catalysis. Inspired by the coordination environment of homogeneous Fe catalysts, we have built the Fe-N_2 single-atom sites on carbon nitride (Fe-N_2/CN), which could catalyze the decarboxylative Giese reactions via radical–radical cross-coupling (Fig. 1(d)). Apart from the Fe-N_2/CN and solvent, this reaction achieves excellent yields (up to 99%) without any additives, outperforming other homogeneous Fe complexes. The Fe-N_2 single-atom sites are the key to catalyze the LMCT process, which could achieve the decarboxylation of alkyl acids to C-centered radicals. Moreover, the carbon nitride (g-C_3N_4) could also be excited by light, promoting the oxidation from Fe(II) back to Fe(III) and reduction activation of electron-deficient olefins to corresponding radical anion. Hence, this SASC has both LMCT and SET activity. We believe that the structural design and catalytic mechanism of SASCs could be inspired by molecular catalysts, expanding the application scenarios of heterogeneous photocatalysts.

2 Experimental

2.1 Materials

The urea, iron(III) acetylacetonate, dichloromethane, alkyl carboxylic acids, and olefins were purchased from Shanghai Aladdin Biochemical Technology Co., Ltd. (China), Bide Pharmatech Ltd. (China), or J&K Scientific Co., Ltd. (China). The light-emitting diode (LED) reactors were purchased from Wuhan Shangjiukeji Co., Ltd. (China). All reagents were used directly without purification.

2.2 Catalyst preparation

The preparation process of g-C_3N_4: 40 g urea was put into crucible and then the crucible was moved into a Muffle furnace. The urea was heated to 550 °C at a heating rate of 0.5 °C/min, held for 2 h. After cooling down to room temperature, carbon nitride was obtained as light-yellow solid powder.

The preparation process of Fe-N_2/CN: Firstly, 400 mg carbon nitride and 100.9 mg Fe(acac)$_3$ were added in 20 mL CH_2Cl_2 and the mixture was stirred vigorously for 5 h. And then, the precursor solution was transferred to a 250 mL beaker and placed in a fume hood to completely volatilize CH_2Cl_2. The solid mixture and 100 mL deionized water was added into a photo reactor and irradiated with a xenon lamp for 5 h. Finally, through filtration, washing and drying, the single-atom Fe-N_2/CN photocatalyst was obtained.

2.3 Photocatalytic decarboxylative Giese reactions

The cyclohexanecarboxylic acid (**1a**, 0.4 mmol, 2.0 equiv.),

benzylidenemalononitrile (**2a**, 0.2 mmol, 1.0 equiv.) and Fe-N_2/CN photocatalyst (10 mg) were added into a Schlenk tube. And then the tube was charged with nitrogen gas. Finally, toluene (1.5 mL) was added. The reaction mixture was stirred and irradiated by a commercially available single wavelength ultraviolet LED (365 nm) for 48 h. After quenching by ethyl acetate (5 mL), the photocatalyst was extracted and filtered to achieve solid–liquid separation.

The aqueous phase was extracted with ethyl acetate (3 × 15 mL) and the combined organic layers were dried over Na_2SO_4 and filtered. The filtrate was concentrated in vacuo and purified by flash column chromatography eluting with petroleum ether/ethyl acetate (EtOAc) to obtain desired product.

The detailed performance of catalysts and experiment procedures are described in the Electronic Supplementary Material (ESM).

3 Result and discussion

3.1 Characterization of Fe-N_2/CN

The design and construction of single-atom photocatalyst are mainly based on the coordination anchoring of Fe atoms by the lone pair electrons of abundant N atoms in the carbon nitride skeleton (Fig. 2(a)). The ligand exchange reaction could be promoted by light irradiation, which is called the photo-induced ligand exchange (PILE) strategy [40]. The inductively coupled plasma-emission spectrometry (ICP-OES) results showed that the loading amount of Fe was 2.2 wt.% (Table S1 in the ESM). Energy-dispersive X-ray spectroscopy (EDX) elemental mappings (Fig. 2(b)) exhibited that the Fe element was homogeneously dispersed on the g-C_3N_4 (Fig. 2(d)). The individual bright dots could be detected by the aberration-corrected high-angle annular dark-field scanning transmission electron microscopy (AC HAADF-STEM) (Fig. 2(c)). This indicated that at the microscopic level, the Fe species did not undergo agglomeration but rather remained atomically dispersed. Synchrotron X-ray absorption spectroscopy (XAS) results confirmed the valence state and coordination environment of Fe species. In the Fe K-edge X-ray absorption near-edge structure (XANES) spectra, the pre-edge of Fe-N_2/CN indicated the oxidation state of iron in Fe-N_2/CN may lie between +2 and +3. Hence, this catalyst contained both Fe(II) and Fe(III) (Fig. 2(d)). In R-space of extended X-ray absorption fine structure

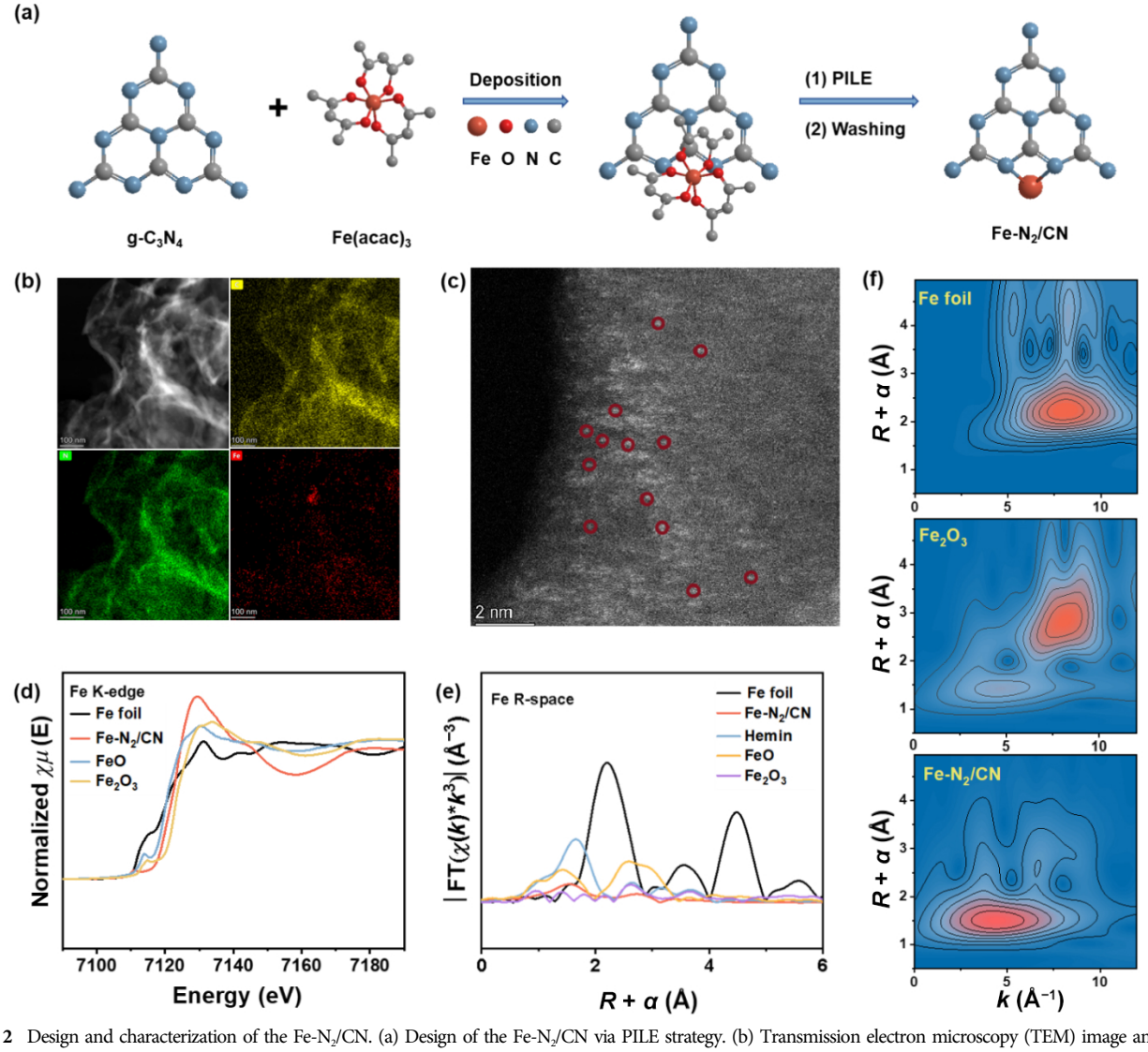

Figure 2 Design and characterization of the Fe-N_2/CN. (a) Design of the Fe-N_2/CN via PILE strategy. (b) Transmission electron microscopy (TEM) image and EDX elemental mappings. (c) AC HAADF-STEM image. (d) The XANES and (e) Fourier transform (FT)-EXAFS spectra. (f) The wavelet transforms for EXAFS.

(EXAFS) spectra, the first coordination shell of Fe–N could be detected, without Fe–Fe coordination peaks (Fig. 2(e)). The EXAFS fitting results indicated that the coordination number was 2, which imply the existence of Fe-N_2 sites (Table S2 in the ESM). The X-ray photoelectron spectroscopy (XPS) spectrum of Fe 2p (at 711 eV and 724 eV) indicated the existence of both Fe(III) and Fe (II) species (Fig. S3 in the ESM), which was consistent with XAS results. Figure 2(f) shows the intensity maximum of wavelet transforms in different Fe species. The 4.4 $Å^{-1}$ in Fe-N_2/CN could be caused by Fe–N bonds. The feature peaks at 2θ = 27.6° (002) and 12.8° (210) were detected by X-ray diffraction (XRD) analysis both in Fe-N_2/CN and g-C_3N_4 (Fig. S4 in the ESM). Using the ultraviolet–visible (UV–vis) spectra (Fig. S5 in the ESM) and valence band XPS spectra (Fig. S6 in the ESM), the energy band structure of Fe-N_2/CN has been clarified, which was as same as that of g-C_3N_4. These results indicated that the introduction of Fe single-atom sites did not change the skeleton of g-C_3N_4. In transient photocurrent tests (Fig. S7 in the ESM), the Fe-N_2/CN showed a higher photocurrent density (10 $\mu A \cdot cm^{-2}$) under light irradiation, implying that Fe single-atom sites could promote the carrier migration.

3.2 Fe-N_2/CN catalyzed decarboxylative Giese reactions

After clarifying the structure of Fe-N_2/CN, it has been used to realize the decarboxylative Giese reactions between cyclohexanecarboxylic acid (**1a**) and 2-benzylidenemalononitrile (**2a**) under irradiation of 365 nm LEDs (Fig. 3). Under the standard conditions, only the Fe-N_2/CN catalyst and solvent were necessary besides substrates, and the Giese radical addition product (**3aa**) could be obtained with 99% yield. Through the control experiments, the light irradiation was necessary. When using g-C_3N_4 instead of Fe-N_2/CN, the yield would decrease to 4%, implying that only through the SET process it is hard to activate the alkyl acid. Using homogeneous $FeCl_3$ as the catalyst instead of Fe-N_2/CN, the yield would reduce significantly to 21%. And then, we added four kinds of homogeneous ligand with 2–4 ligating N atoms into reaction systems with $FeCl_3$, respectively. The bipyridine yielded the optimal results ($FeCl_3$+L1, 62% yield). This indicates that Fe–N_2 coordination might be the most favorable for LMCT, which was consistent with single-atom catalysis. And we measured the initial reaction rate and obtained that the apparent quantum yield (AQY) was 0.66% (Fig. S13 in the ESM).

Subsequently, we conducted cycling experiments and observed that the initial reaction rate decreased significantly in the third cycle (Fig. S14 in the ESM). Through ICP-OES analysis, we determined that the decline in yield was due to Fe leaching. Hence, we used the PILE strategy again for reloading Fe onto the recycled catalyst, which restored its catalytic activity. Therefore, for Fe-N_2/CN, only the ligand (carbon nitride) is recyclable and reusable.

3.3 Mechanism investigations

At first, the light on/off tests indicated that the continuous illumination was necessary, excluding the radical chain reaction (Fig. 4(a)). Through Stern–Volmer experiments, the electron transfer pathway between excited-state Fe-N_2/CN and substrates has been proved (Fig. 4(b)). The excited-state Fe-N_2/CN could be quenched by both Fe(II) and **2a**, but could not be quenched by **1a**. These results implied that Fe(II) could be oxidized to Fe(III) by the hole of g-C_3N_4, and the photogenerated electron could reduce **2a**. Notably, there was no direct electron transfer between **1a** and excited-state g-C_3N_4. It indicated that the hole of g-C_3N_4 could not oxidize **1a** and realize the decarboxylation. Through the electron paramagnetic resonance (EPR) spin-trapping test with 5,5-dimethyl-1-pyrroline-*N*-oxide (DMPO), the radical intermediate could be

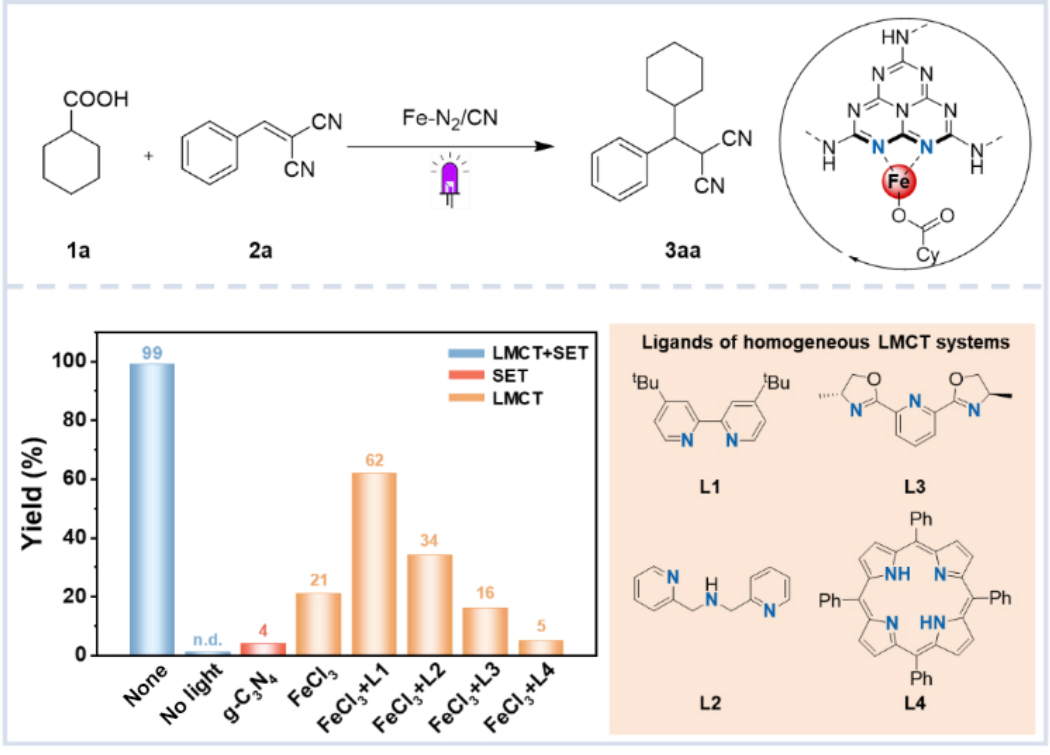

Figure 3 Fe-N_2/CN catalyzed decarboxylative Giese reactions and control experiments. Standard conditions: **1a** (2 equiv., 0.4 mmol), **2a** (1 equiv., 0.2 mmol), Fe-N_2/CN (10 mg), toluene (1.5 mL), rt, N_2, 48 h, 365 nm LEDs. 5 mol% Fe salts and ligands were used for comparation with single-atom catalytic systems.

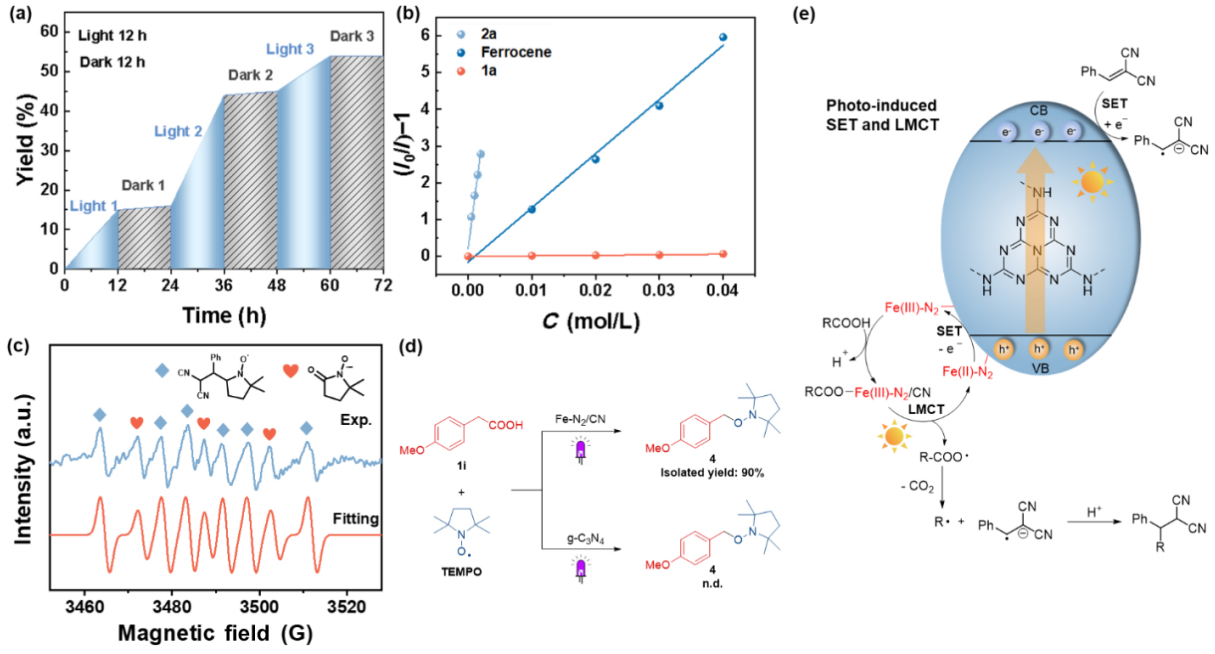

Figure 4 Mechanism investigation of decarboxylative Giese reactions. (a) Time profiles of decarboxylative Giese reaction with and without light. (b) Fe-N_2/CN emission quenching with **1a**, **2a**, and ferrocene. (c) EPR analysis with DMPO and fitting results. Conditions: **2a** (1 equiv., 0.2 mmol), Fe-N_2/CN (10 mg), DMPO (1 equiv., 0.2 mmol), toluene (1.5 mL), rt, N_2, 1 h, 365 nm LEDs. C-centered radical: A_N = 14.02 G, A_H = 19.62 G. Oxidative product of DMPO: A_N = 15.22 G. (d) TEMPO trapping experiments. Conditions: **3i** (1 equiv., 0.2 mmol), TEMPO, 2,2,6,6-tetramethyl-1-piperidinyloxy (2.5 equiv., 0.5 mmol), photocatalyst (10 mg, Fe-N_2-CN or g-C_3N_4), toluene (1.5 mL), rt, N_2, 48 h, 365 nm LEDs. (e) Proposed mechanism.

trapped and detected. When only **2a** was added without **1a** under standard reaction conditions, a carbon-centered radical could be captured by DMPO (A_N = 14.02 G, and A_H = 19.62 G), implying the radical anion of **2a**. And the oxidative product of DMPO showed a triplet peak (Fig. 4(c)). Further control experiments revealed that the addition of hole (TEA) or electron sacrificial agents ($AgNO_3$) markedly inhibited the reaction (Table S3 in the ESM). This indicated that both the oxidation by holes and the reduction by photogenerated electrons were essential in the reaction process. The radical inhibitors, (2,2,6,6-tetramethylpiperidin-1-yl)oxyl or (2,2,6,6-tetramethylpiperidin-1-yl)oxidanyl (TEMPO) and butylated hydroxytoluene (BHT), could completely suppress the reaction (Table S3 in the ESM). These results indicated that the radical should be the key intermediate. And the radical/radical cross-coupling product between benzyl radical and TEMPO could be obtained with 90% isolated yield (Fig. 4(d)). If using g-C_3N_4 instead of Fe-N_2/CN, the benzyl radical could not be trapped. This implied that the Fe sites were the key for the decarboxylation.

To sum up, the proposed mechanism is shown in Fig. 4(e). At first, Fe(II) could be oxidized to Fe(III) by the hole of carbon nitride. After the carboxyl group coordinates with Fe(III), the Fe–O bond homolysis was promoted by light irradiation to produce corresponding O-centered radical and Fe(II). Through the decarboxylation, the corresponding alkyl radical could be obtained. Meanwhile, the photogenerated electron could reduce **2a** to radical anion. In this way, the electron-deficient olefins could be activated. Through the radical/radical cross-coupling between alkyl radical and radical anion, the new C–C bond could be formed. The LMCT and SET catalytic cycles could be merged and operate smoothly in this Fe-N_2/CN catalytic system.

3.4 Substrate scope

Under optimal conditions, we have explored the substrate scope of decarboxylative Giese reactions (Fig. 5). Secondary cyclic carboxylic acids could afford the corresponding products in moderate to good yields (**3aa**, **3ba**, **3ca**). For 2,3-dihydro-1H-indene-1-carboxylic acid, the yield would decrease to 43% (**3da**). We proposed that the conjugated effect reduced the delocalization index of C-centered radical, making it less prone to undergo radical addition with the alkene. Tertiary cyclic carboxylic acids show good yields (**3ea**, **3fa**, **3ga**), and the cyclopropyl group could be reserved (**3ga**). The chain tertiary carboxylic acid (**3ha**) affords a moderate yield. The phenylacetic acid derivatives (**3ia**, **3ja**) have good compatibility, including ibuprofen with a 99% yield (**3ka**). The presence of electron-donating groups on the benzene ring could increase the electron density, resulting in a significant improvement in yield. For chain primary carboxylic acids, the corresponding products could not be detected (Fig. S13 in the ESM). We proposed that the radical stability was the key for obtaining good yield. Primary carbon radicals generally exhibited low stability. When olefins become relatively electron-rich, the yields will decrease accordingly (**3ib**, **3ic**). Through Stern–Volmer experiments, the styrene exhibited negligible quenching of the excited-state carbon nitride, indicating that electrons in the conduction band cannot reduce styrene to the radical anion (Fig. S15 in the ESM). These results suggested that the single-electron reduction of the alkene was crucial for promoting the Giese reaction in this system. Hence, only the electron-deficient olefins can obtain corresponding products. Moreover, the C–N bond could form through the similar decarboxylative Giese reactions (**3id**).

4 Conclusions

In summary, we have built Fe-N_2 single-atom sites on carbon nitride via the photo-induced ligand exchange strategy. Under light irradiation, the ligand-to-metal electron transfer could achieve from

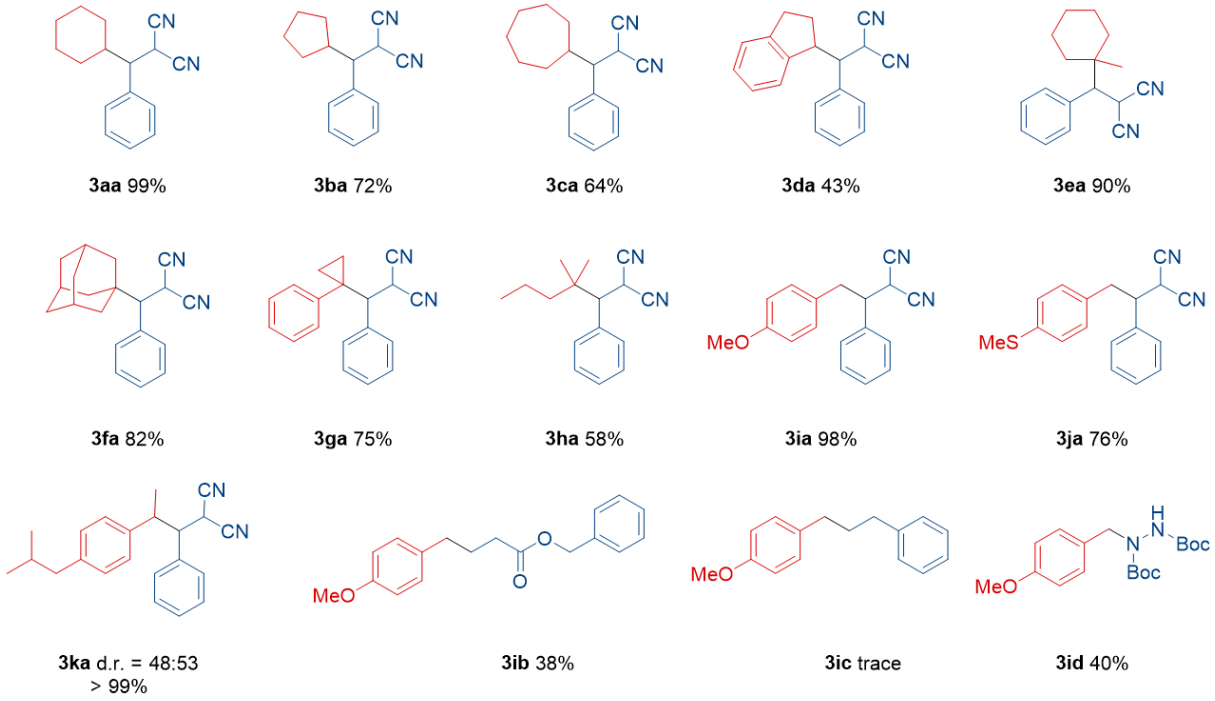

Figure 5 Substrate scope under standard conditions. Standard conditions: 1 (2 equiv., 0.4 mmol), 2 (1 equiv., 0.2 mmol), Fe-N_2/CN (10 mg), toluene (1.5 mL), rt, N_2, 48 h, 365 nm LEDs.

carboxylic acid to Fe-N_2 sites, and the decarboxylative Giese reaction can be realized smoothly. Notably, by constructing a similar coordination structure of homogeneous metal complexes, the single-atom sites may exhibit analogous structure–activity relationships. It implies that single-atom catalysts might bridge the homo- and heterogeneous catalytic system and offers a new opportunity to achieve organic transformations.

Electronic Supplementary Material: Supplementary material (including the experimental procedure, characterization data, and copies of ^{1}H and ^{13}C spectra) is available in the online version of this article at https://doi.org/10.26599/NR.2026.94908469.

Data availability

All data needed to support the conclusions in the paper are presented in the manuscript and the Electronic Supplementary Material. Additional data related to this paper may be requested from the corresponding author upon request.

Acknowledgements

This study was financially supported by the National Natural Science Foundation of China (Nos. 22272003, 22301013, 22579008, and 22502012), the Beijing Natural Science Foundation (No. Z250018), the National Key R&D Program of China (No. 2023YFB3810800), the R&D Program of Beijing Municipal Education Commission (No. KZ20231000506), and the Project of Construction of Innovative Teams and Teacher Career Development for Universities and Colleges Under Beijing Municipality (No. 11000024T000003219982). We would like to thank the Shanghai Synchrotron Radiation Facility of BL11B (https://cstr.cn/31124.02.SSRF.BL11B) and Beijing Synchrotron Radiation Facility (BSRF) 1W1B beamline for the assistance on XAS measurements, Large-scale Instruments and Equipment Sharing Platform (BJUT) for GC-MS, NMR testing.

Declaration of competing interest

All the contributing authors report no conflict of interests in this work.

Author contribution statement

Y. J.: Methodology, validation, formal analysis, data curation, investigation, writing. G. L. W.: Formal analysis, data curation, investigation. M. L. M.: Formal analysis, data curation, investigation. J. M. W.: Formal analysis, data curation, investigation. L. A.: Investigation. D. Q.: Investigation, funding acquisition. K. Z.: Investigation. P. J. M.: Supervision, formal analysis, data curation, investigation. Y. C. L.: Writing, supervision, conceptualization, validation, project administration, funding acquisition. Z. C. S.: Writing, supervision, conceptualization, resources, validation, project administration, funding acquisition. All the authors have approved the final version of the manuscript.

Use of AI statement

None.

References

[1] Chan, A. Y.; Perry, I. B.; Bissonnette, N. B.; Buksh, B. F.; Edwards, G. A.; Frye, L. I.; Garry, O. L.; Lavagnino, M. N.; Li, B. X.; Liang, Y. F. et al. Metallaphotoredox: The merger of photoredox and transition metal catalysis. *Chem. Rev.* **2022**, *122*, 1485–1542.

[2] Savateev, A.; Ghosh, I.; König, B.; Antonietti, M. Photoredox catalytic organic transformations using heterogeneous carbon nitrides. *Angew. Chem., Int. Ed.* **2018**, *57*, 15936–15947.

[3] Huang, C.; Li, X. B.; Tung, C. H.; Wu, L. Z. Photocatalysis with quantum dots and visible light for effective organic synthesis. *Chem. —Eur. J.* **2018**, *24*, 11530–11534.
[4] Zhu, Y. Y.; He, Y. Y.; Li, Y. X.; Liu, C. H.; Lin, W. B. Heterogeneous porous synergistic photocatalysts for organic transformations. *Chem. —Eur. J.* **2024**, *30*, e202400842.
[5] Cabanero, D. C.; Rovis, T. Low-energy photoredox catalysis. *Nat. Rev. Chem.* **2025**, *9*, 28–45.
[6] Zhao, E.; Zhang, W. J.; Dong, L.; Zbořil, R.; Chen, Z. P. Photocatalytic transfer hydrogenation reactions using water as the proton source. *ACS Catal.* **2023**, *13*, 7557–7567.
[7] Wang, J. M.; Liu, Y. C.; Zong, X. P.; Lei, A. W.; Sun, Z. C. Recent advances in the heterogeneous photochemical synthesis of C–N bonds. *Green Chem.* **2023**, *25*, 5010–5023.
[8] Prier, C. K.; Rankic, D. A.; MacMillan, D. W. C. Visible light photoredox catalysis with transition metal complexes: Applications in organic synthesis. *Chem. Rev.* **2013**, *113*, 5322–5363.
[9] Shaw, M. H.; Twilton, J.; MacMillan, D. W. C. Photoredox catalysis in organic chemistry. *J. Org. Chem.* **2016**, *81*, 6898–6926.
[10] Romero, N. A.; Nicewicz, D. A. Organic photoredox catalysis. *Chem. Rev.* **2016**, *116*, 10075–10166.
[11] Liu, X. L.; Zhang, Q. Z.; Ma, D. L. Advances in 2D/2D Z-scheme heterojunctions for photocatalytic applications. *Solar RRL* **2021**, *5*, 2000397.
[12] Xu, Q. L.; Zhang, L. Y.; Cheng, B.; Fan, J. J.; Yu, J. G. S-scheme heterojunction photocatalyst. *Chem* **2020**, *6*, 1543–1559.
[13] Xue, J. W.; Fujitsuka, M.; Tachikawa, T.; Bao, J.; Majima, T. Charge trapping in semiconductor photocatalysts: A time- and space-domain perspective. *J. Am. Chem. Soc.* **2024**, *146*, 8787–8799.
[14] Qin, J.; Lei, H.; Gao, C. H.; Zheng, Y. W.; Zhao, Y. T.; Xia, W. J. Light-induced ligand-to-metal charge transfer of Fe(III)-OR species in organic synthesis. *Org. Biomol. Chem.* **2024**, *22*, 6034–6044.
[15] May, A. M.; Dempsey, J. L. A new era of LMCT: Leveraging ligand-to-metal charge transfer excited states for photochemical reactions. *Chem. Sci.* **2024**, *15*, 6661–6678.
[16] An, Q.; Chang, L.; Pan, H.; Zuo, Z. W. Ligand-to-Metal Charge Transfer (LMCT) catalysis: Harnessing simple cerium catalysts for selective functionalization of inert C–H and C–C bonds. *Acc. Chem. Res.* **2024**, *57*, 2915–2927.
[17] Chaudhuri, A.; Denkler, L. M.; Zhuo, Q.; Mandal, A.; Bunescu, A. LMCT-driven iron photocatalysis: Mechanistic insights and synthetic applications. *Chem. —Eur. J.* **2025**, *31*, e02185.
[18] Patra, T.; Maiti, D. Decarboxylation as the key step in C−C bond-forming reactions. *Chem. —Eur. J.* **2017**, *23*, 7382–7401.
[19] Kitcatt, D. M.; Nicolleb, S.; Lee, A. L. Direct decarboxylative Giese reactions. *Chem. Soc. Rev.* **2022**, *51*, 1415–1453.
[20] Giese, B. Formation of CC bonds by addition of free radicals to alkenes. *Angew. Chem., Int. Ed.* **1983**, *22*, 753–764.
[21] Komeyama, K.; Michiyuki, T.; Teshima, Y.; Osaka, I. Visible light-driven Giese reaction with alkyl tosylates catalysed by nucleophilic cobalt. *RSC Adv.* **2021**, *11*, 3539–3546.
[22] Patra, T.; Mukherjee, S.; Ma, J. J.; Strieth-Kalthoff, F.; Glorius, F. Visible-light-photosensitized aryl and alkyl decarboxylative functionalization reactions. *Angew. Chem., Int. Ed.* **2019**, *58*, 10514–10520.
[23] Ji, C. L.; Lu, Y. N.; Xia, S. Y.; Zhu, C. J.; Zhu, C. Q.; Li, W. P.; Xie, J. Photoinduced late-stage radical decarboxylative and deoxygenative coupling of complex carboxylic acids and their derivatives. *Angew. Chem., Int. Ed.* **2025**, *64*, e202423113.
[24] He, S. Q.; Li, H. C.; Chen, X. L.; Krylov, I. B.; Terent'ev, A. O.; Qu, L. B.; Yu, B. Advances of *N*-hydroxyphthalimide esters in photocatalytic alkylation reactions. *Chin. J. Org. Chem.* **2021**, *41*, 4661–4689.
[25] Lu, J. Q.; Yao, Y.; Li, L. B.; Fu, N. K. Dual transition metal electrocatalysis: Direct decarboxylative alkenylation of aliphatic carboxylic acids. *J. Am. Chem. Soc.* **2023**, *145*, 26774–26782.
[26] Lai, X. L.; Chen, M.; Wang, Y. Q.; Song, J. S.; Xu, H. C. Photoelectrochemical asymmetric catalysis enables direct and enantioselective decarboxylative cyanation. *J. Am. Chem. Soc.* **2022**, *144*, 20201–20206.
[27] Li, Q. Y.; Gockel, S. N.; Lutovsky, G. A.; DeGlopper, K. S.; Baldwin, N. J.; Bundesmann, M. W.; Tucker, J. W.; Bagley, S. W.; Yoon, T. P. Decarboxylative cross-nucleophile coupling via ligand-to-metal charge transfer photoexcitation of Cu(II) carboxylates. *Nat. Chem.* **2022**, *14*, 94–99.
[28] Pedersen, P. S.; Blakemore, D. C.; Chinigo, G. M.; Knauber, T.; MacMillan, D. W. C. One-pot synthesis of sulfonamides from unactivated acids and amines via aromatic decarboxylative halosulfonylation. *J. Am. Chem. Soc.* **2023**, *145*, 21189–21196.
[29] Crocker, M. S.; Lin, J. Y.; Nsouli, R.; McLaughlin, N. D.; Musaev, D. G.; Mehranfar, A.; Lopez, E. R.; Ackerman-Biegasiewicz, L. K. G. Transformative ligand effects in Fe-photocatalyzed Giese-type additions. *Chem Catal.* **2024**, *4*, 101131.
[30] Qian, J. H.; Zhang, Y.; Zhao, W. N.; Hu, P. Decarboxylative halogenation of aliphatic carboxylic acids catalyzed by iron salts under visible light. *Chem. Commun.* **2024**, *60*, 2764–2767.
[31] Fernández‐García, S.; Chantzakou, V. O.; Juliá-Hernández, F. Direct decarboxylation of trifluoroacetates enabled by iron photocatalysis. *Angew. Chem., Int. Ed.* **2024**, *63*, e202311984.
[32] Li, Z. L.; Wang, X. F.; Xia, S. Q.; Jin, J. Ligand-accelerated iron photocatalysis enabling decarboxylative alkylation of heteroarenes. *Org. Lett.* **2019**, *21*, 4259–4265.
[33] Xia, S. Q.; Hu, K. J.; Lei, C. H.; Jin, J. Intramolecular aromatic C–H acyloxylation enabled by iron photocatalysis. *Org. Lett.* **2020**, *22*, 1385–1389.
[34] Yan, N.; Wang, Y.; Bao, M.; Yu, X. Q. Visible-light-driven iron-catalyzed atom transfer radical addition of CH_2Br_2 to alkenes: Facile access to 1,3-dibromo compounds. *Angew. Chem., Int. Ed.* **2025**, *64*, e202511486.
[35] Qi, X. K.; Yao, L. J.; Zheng, M. J.; Zhao, L. L.; Yang, C.; Guo, L.; Xia, W. J. Photoinduced hydrodifluoromethylation and hydromethylation of alkenes enabled by ligand-to-iron charge transfer mediated decarboxylation. *ACS Catal.* **2024**, *14*, 1300–1310.
[36] Zhang, L. L.; Yang, X. F.; Lin, J.; Li, X. N.; Liu, X. Y.; Qiao, B. T.; Wang, A. Q.; Zhang, T. On the coordination environment of single-atom catalysts. *Acc. Chem. Res.* **2025**, *58*, 1878–1892.
[37] Liang, X.; Yao, S. C.; Li, Z.; Li, Y. D. Challenge and chance of single atom catalysis: The development and application of the single atom site catalysts toolbox. *Acc. Chem. Res.* **2025**, *58*, 1607–1619.
[38] Wu, X.; Zhang, H. B.; Zuo, S. W.; Dong, J. C.; Li, Y.; Zhang, J.; Han, Y. Engineering the coordination sphere of isolated active sites to explore the intrinsic activity in single-atom catalysts. *Nano-Micro Lett.* **2021**, *13*, 136.
[39] Cui, X. J.; Li, W.; Ryabchuk, P.; Junge, K.; Beller, M. Bridging homogeneous and heterogeneous catalysis by heterogeneous single-metal-site catalysts. *Nat. Catal.* **2018**, *1*, 385–397.
[40] Wang, G. L.; Liu, Y. C.; Zhang, X. Y.; Zong, X. P.; Zhang, X.; Zheng, K.; Qu, D.; An, L.; Qi, X. T.; Sun, Z. C. Mechanistic investigation into single-electron oxidative addition of single-atom Cu(I)−N_4 site: Revealing the Cu(I)−Cu(II)−Cu(I) catalytic cycle in photochemical hydrophosphinylation. *J. Am. Chem. Soc.* **2024**, *146*, 8668–8676.